

**Supplementary Material for**

**Structural conversion of neurotoxic amyloid- $\beta$ (1-42) oligomers to fibrils**

Mahiuddin Ahmed<sup>1</sup>, Judianne Davis<sup>2</sup>, Darryl Aucoin<sup>1</sup>, Takeshi Sato<sup>3</sup>, Shivani Ahuja<sup>4</sup>, Saburo Aimoto<sup>3</sup>, James I. Elliott<sup>5</sup>, William E. Van Nostrand<sup>2</sup> and Steven O. Smith<sup>1</sup>

*<sup>1</sup>Departments of Biochemistry and Cell Biology, <sup>2</sup>Neurosurgery and Medicine, <sup>4</sup>Physics and Astronomy, Stony Brook University, Stony Brook, New York 11794-5215. <sup>3</sup>Institute for Protein Research, Osaka University, 3-2 Yamadaoka, Suita, Osaka 565-0871, Japan. <sup>5</sup>Department of Molecular Biophysics and Biochemistry, Yale University, New Haven, Connecticut 06520*

Correspondence should be addressed to S.O.S. ([steven.o.smith@sunysb.edu](mailto:steven.o.smith@sunysb.edu)).

## Supplementary Results 1: Models of A $\beta$ 42 Oligomers and Fibrils.

Molecular models of A $\beta$ 42 oligomers and fibrils (**Supplementary Fig. 1**) were developed by combining the results of solid-state and solution NMR spectroscopy, Fourier transform infrared (FTIR) spectroscopy, size exclusion chromatography (SEC), and single-touch atomic force microscopy (AFM).

### **A $\beta$ 42 Oligomers**

The soluble neurotoxic oligomers stabilized at 4 °C and low salt are composed primarily of pentamers and possibly hexamers. Native gels and SEC (see **Supplementary Results 3**) are consistent with a homogeneous population of oligomers with a molecular weight of ~24 kDa  $\pm$  3 kDa. **Supplementary Figure 1b** presents a model of the oligomer complex illustrating that the molecular volume of five loosely packed monomers of A $\beta$ 42 occupy the molecular volume obtained from an analysis of the oligomers imaged by single touch AFM (see **Supplementary Results 2**).

Simulations of the A $\beta$ 42 monomer in the oligomer complex (**Supplementary Fig. 1a**) predict two distinct surfaces. One surface is largely hydrophobic, while the opposite face is more polar and dominated by charged groups at the N-terminus. These monomer units may then form pentamer/hexamer complexes. If the interactions are symmetric around the central pentamer axis, then one face of the pentamer will be largely hydrophobic (as in **Supplementary Fig. 1b**) and the opposite face will be appreciably more polar.

**Supplementary Figure 1b** shows the side view of the pentamer complex of A $\beta$ 42. The predicted 2 nm height is consistent with the 2.2 nm average height obtained from AFM (see **Supplementary Fig. 3**). The height measurement is extremely accurate ( $\pm$  0.1 nm) in AFM. The model predicts an indentation in the middle of the surface. This centrosymmetric structure has been observed in **Figure 6c (main text)** and previously by others in A $\beta$ 40 (see *Lashuel et al.*<sup>1</sup>). Whether these oligomers form membrane channels, however, remains an open question.

**Supplementary Figure 1c** presents a model of a decamer (side view). The height of the decamer is ~4 nm. We suggest that the hydrophobic faces of two pentamers can associate to form a decamer (or a dodecamer for the association of two hexameric oligomers). There is evidence for dodecamer assemblies of A $\beta$ 42<sup>2-4</sup>.

There are several particles in the AFM images shown in **Supplementary Figure 2** with heights of 3-4 nm, but with the same lateral dimensions (i.e. diameters) as particles with 2 nm heights. This observation suggests that particles with 4 nm heights result from stacking of particles with 2 nm heights. This interpretation of the AFM images argues that the oligomers are disc-shaped particles rather than spherical micelles that have been flattened upon binding to

the mica surface. Our previous single-touch AFM images of soluble A $\beta$ 42 oligomers (see Fig. 6 in *Mastrangelo et al.*<sup>5</sup>) reveal that disc-shaped particles with the dimensions similar to those in **Supplementary Figure 1c** are readily obtained at physiological temperature and salt. We now interpret these “high molecular weight” oligomers as decamers/dodecamers. In fact, we found that peptide inhibitors are able to cap the oligomers at a 2.8 nm average height without changing their observed width<sup>5</sup>. The amphipathic peptide inhibitors may prevent decamer assembly by binding to the hydrophobic face of the pentamer.

Recent results using analytical mass spectrometry to investigate oligomer size distributions found that only hexamers and dodecamers were formed by A $\beta$ 42<sup>6</sup>. Additional hexamer units did not add to the dodecamer to form 18-mers, and the formation of dodecamers from hexamers did not involve the addition of monomer or dimer units. These observations are consistent with the dimerization or stacking of hexamers (or pentamers) as described above. In our model, the interaction of the two hydrophobic surfaces of the hexamer caps the growth of the dodecamers.

The model of the pentamer with a large hydrophobic surface is consistent with results from urea denaturation and Bis-ANS binding studies<sup>7</sup>. One of the most striking differences in A $\beta$ 40 and A $\beta$ 42 oligomers is the ability of the oligomer to bind Bis-ANS. There is a 10-fold increase in binding of Bis-ANS to A $\beta$ 42 in the oligomeric state over denatured A $\beta$ 42 indicating that the folded structure has a distinct hydrophobic surface. Also, urea has been shown to denature the oligomers, but does not prevent fibril formation. This observation suggests that the oligomers are not an obligate intermediate in fibril formation. Rather, the oligomers appear to adopt a stable, folded conformation and must unfold prior to refolding into the parallel and in-register geometry characteristic of fibrils.

### ***Molecular Dynamics Simulations of the A $\beta$ 42 Monomer in the Oligomer Conformation***

The structural constraints obtained by solid-state and solution NMR spectroscopy, along with the information on the size and molecular composition of the A $\beta$ 42 oligomers from SEC, native gels and light scattering, can be used to restrain and evaluate molecular models of the A $\beta$ 42 oligomer (e.g. see *Urbanc et al.*<sup>8</sup>, *Yun et al.*<sup>9</sup>, and *Nguyen et al.*<sup>10</sup>). **Supplementary Figure 1a** presents a molecular model of the monomer unit in the A $\beta$ 42 oligomer obtained by restrained molecular dynamics simulations and energy minimization using Discovery Studio 2.5 (Accelrys, San Diego, CA). A standard dynamics cascade was implemented using the CHARMM force field with a two stage steepest descent and conjugate gradient minimization, followed by heating and equilibration.

Restraints based on solid-state NMR distance measurements and solution state NMR amide H/D exchange measurements were placed on a starting extended structure of A $\beta$ 42. A restraint ( $\leq 5$  Å) was placed between the side chain positions of Phe19-(C $\zeta$ ) and Leu34 (C $\delta$ ) corresponding to the restraint obtained from our solid-state NMR measurement. Two additional

restraints were included between the backbone nitrogens of Val12 and Leu17 (10 Å) and between Val36 and Val39 (6 Å) on the basis of amide H-D exchange (**Supplementary Fig. 6**). We found that two stretches of amino acids (His13-Gln15 and Gly37-Gly38) were accessible to bulk solvent, but were flanked by regions that were inaccessible. The added restraints generated turns that allowed the adjacent sequences to collapse onto one another. A similar turn region at Gly37-Gly38 was observed in molecular dynamics simulations of A $\beta$ 42 oligomer formation by *Urbanc et al.*<sup>8</sup>. The resulting structure contained one surface that was largely hydrophobic, while the opposite surface was more polar and dominated by charged groups at the N-terminus.

### **A $\beta$ 42 Fibrils**

The solid-state NMR measurements presented in this study show that the hydrophobic core of A $\beta$ 42 fibrils has a  $\beta$ -strand-turn- $\beta$ -strand ( $\beta$ -turn- $\beta$ ) conformation with Gln15 and Phe19 of the N-terminal  $\beta$ -strand in contact with Gly37 and Leu34 of the C-terminal  $\beta$ -strand, respectively. The  $\beta$ -strands are staggered at the Gln15-Gly37 contact, and polymerize in a parallel, in-register orientation. **Supplementary Figures 1d-f** present models for the monomer unit within the fibril, the protofilament, and a cross-section of a mature fibril.

There are three defining structural features of the protofilament: cross- $\beta$  structure, parallel and in-register orientation of the  $\beta$ -strands and staggered packing (domain-swapping) of the  $\beta$ -strands. Experimental data on the A $\beta$ 42 protofilament generally agree on these features. Fiber diffraction studies of A $\beta$  fibrils reveal cross- $\beta$  structure where the individual  $\beta$ -strands polymerize perpendicular to the fibril axis<sup>11</sup>, and both solid-state NMR and EPR measurements have shown that the  $\beta$ -strands within A $\beta$ 42 fibrils have a parallel and in-register orientation<sup>12-14</sup>. The domain swapping feature identified in this study by the intermolecular Gln15-Gly37 contact is consistent with the pairwise mutational studies of Riek and coworkers<sup>15</sup>.

There is disagreement in the structure of the protofilament at the N-terminus (before Gln15) and at the C-terminus (after Gly37). On the basis of solvent exchange measurements Olofsson *et al.*<sup>16</sup> found that the first 10 residues of A $\beta$ 42 are solvent accessible (and possibly unstructured), whereas similar experiments by Riek and coworkers<sup>15</sup> found that in the first 17 residues, the amide N-H protons in approximately half of the population exchanged quickly ( $\geq 10$  h<sup>-1</sup>), whereas the other half exchanged slowly ( $\leq 10^{-2}$  h<sup>-1</sup>). The interaction of the N-terminus (see below) with the  $\beta$ -turn- $\beta$  core of the protein may explain the slowly exchanging population.

There are also differences in A $\beta$ 42 fibril models after Gly37. Irie and co-workers<sup>17,18</sup> concluded that the C-terminal  $\beta$ -strand breaks at Gly37/38 to allow Ala42 to contact the side-chain of Met35. They observed a cross-peak in DARR NMR experiments between Met35 and Ala42 in fibrils formed after two days of incubation at 37 °C<sup>17</sup>. These studies were based on their earlier proline scanning experiments where it was found that substitution of proline at

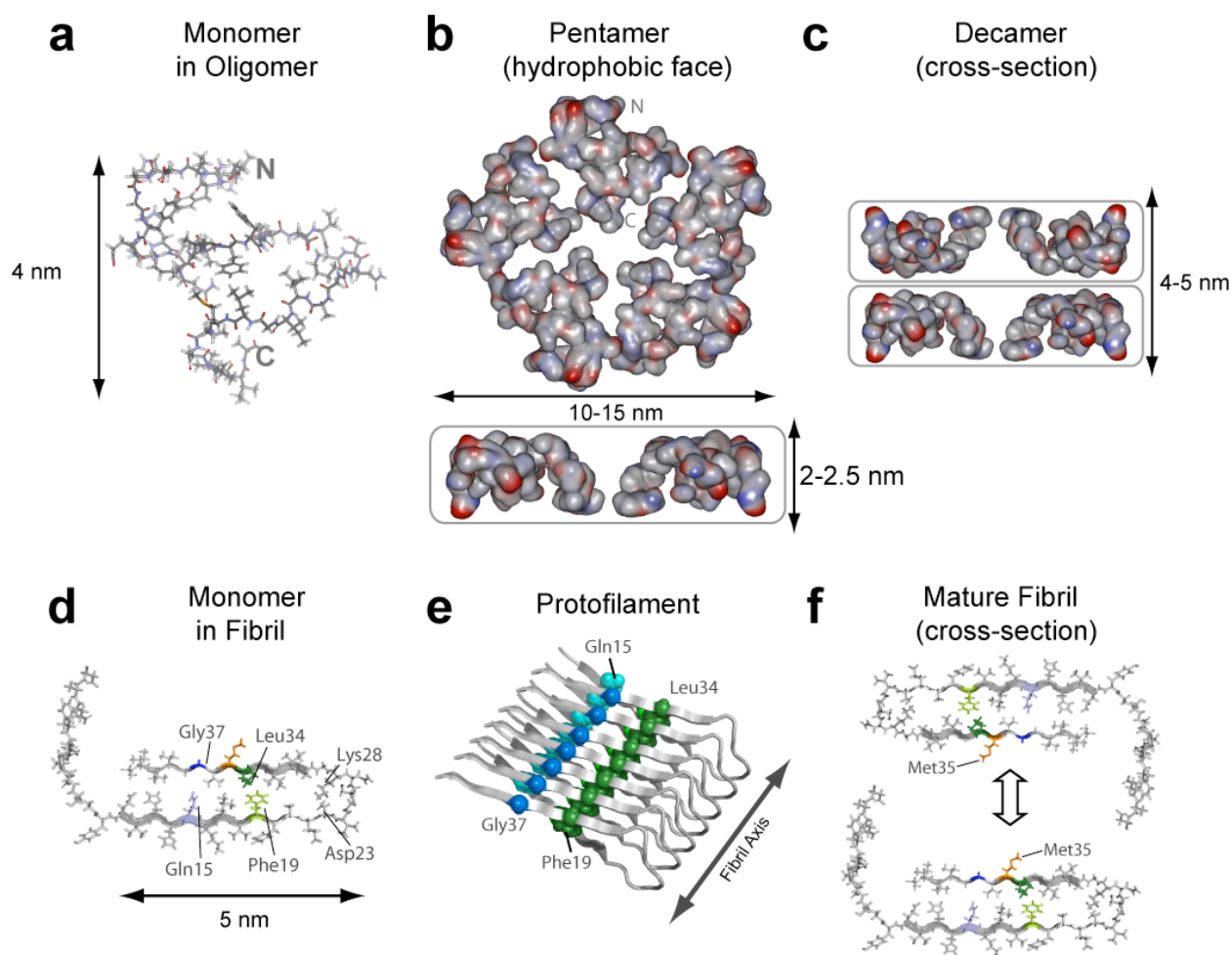
positions 40-42 reduced fibril formation and cytotoxicity, whereas threonine substitutions at residues 41 and 42 aggregated strongly and exhibited potent cytotoxicity.

**Supplementary Figure 1f** presents a model of the mature A $\beta$ 42 fibril. We have previously proposed that the cross section of the A $\beta$ 42 fibril has two protofilaments that form contacts between Met35 and Gly37<sup>19</sup>. Our model of the mature A $\beta$ 42 fibril developed from the observation of this Met35-Gly37 contact also predicts an intermolecular Ile31-Val39 contact between protofilaments. We were unable to observe this contact in our current studies (**Supplementary Results 7**) suggesting that the protofilament interface may be a source of polymorphism in A $\beta$ 42.

In general, polymorphisms in fibril structure might arise from differences in the conditions under which the fibrils are grown. For example, oxidation of Met35 may serve to disrupt hydrophobic interactions between protofilaments. Cryo-EM images of fibrils formed of A $\beta$ 42 with Met35 oxidized show bundles of individual protofilaments each separated by a 15 Å gap<sup>15</sup>. In this case, the unstructured N-terminus may mediate the association of protofilaments to form fibrils. A more recent cryo-EM study of A $\beta$ 42 generated a similar model of the mature fibril<sup>20</sup>. The protofilaments have a  $\beta$ -turn- $\beta$  conformation and a parallel and in-register orientation as in **Supplementary Figure 1e**, and the two protofilaments that form the mature fibril wind around a hollow core as in **Supplementary Figure 1f**. In this reconstruction, the hydrophobic C-terminal sequence of the peptide lines the hollow core and protofilament interactions are mediated by the N-terminal sequence.

The similarities and differences between fibril images observed by TEM and cryo-EM suggest that differences in the experimental conditions (incubation time, buffer conditions, and temperature) may influence fibril morphology. For A $\beta$ 40, there are a number of studies that suggest that the conditions under which the fibrils are grown can produce polymorphisms<sup>21-23</sup>. Tycko and co-workers have provided strong evidence for two well-defined polymorphs<sup>24</sup>, one containing two protofilaments in the fibril cross section and one containing three protofilaments.

For our studies, we typically grow fibrils for at least 10–14 days to observe dense networks of fibrils by TEM. We can monitor the oxidation state of Met35 by the chemical shift of the Met-<sup>13</sup>C $\epsilon$  resonance. Under all of the conditions of our experiments, Met35 remained in the reduced state. While we use low salt concentrations to trap the oligomers, fibrils are grown under physiological conditions (10 mM phosphate, 150 mM NaCl, pH 7.4).



**Supplementary Figure 1.** Molecular models of the A $\beta$ 42 oligomers (a-c) and fibrils (d-f). The model of the A $\beta$ 42 monomer in the oligomer conformation (a) was developed on the basis of structural constraints obtained by solid-state and solution NMR spectroscopy. The constraints were used in restrained molecular dynamics simulations on the A $\beta$ 42 monomer to generate a folded structure. (b) A $\beta$ 42 pentamer. The assembly of five monomers has the dimensions of the most abundant particles observed by AFM. The orientation of the monomer in the model of the pentamer was chosen to place the C-terminus in the center of the oligomer. Hydrogen-deuterium exchange data indicate that the C-terminal three amino acids are among the most protected from solvent exchange. (c) A $\beta$ 42 decamers. The association of disc-shaped pentamers can form decamers with heights of  $\sim 4$  nm. (d) Monomer within the A $\beta$ 42 fibril. The monomer unit has a U-shaped geometry with Phe19 in contact with Leu34. (e) A $\beta$ 42 protofilament. At least two protofilaments associate to form mature fibrils<sup>19</sup>. Our NMR measurements indicate that Gln15 and Gly37 (blue spheres) from adjacent peptides are close in space in the protofilament structure, while pairwise mutational experiments have shown that

Asp23 and Lys28 may interact in adjacent peptides<sup>15</sup>. The Asp23-Lys28 salt bridge is thought to be a key element of the turn structure in A $\beta$ 40<sup>25</sup>. The observation that the Phe19-Leu34 contact in A $\beta$ 42 is the same as in A $\beta$ 40<sup>26</sup> argues that the  $\beta$ -turn- $\beta$  structure is the same in the fibrils formed from these two peptides. A $\beta$ 40 and A $\beta$ 42 can homogeneously co-mix in amyloid fibrils suggesting they have the same structural architecture<sup>14</sup>. (f) Cross section of A $\beta$ 42 fibrils. Two protofilament units can associate to form mature fibrils (shown here in an expanded view since the molecular contacts mediating protofilament association may be a source of polymorphism in A $\beta$ 42 fibrils). We have previously observed that A $\beta$ 42 protofilaments form contacts between Met35 and Gly37<sup>19</sup>. However, a recent cryo-EM study of A $\beta$ 42 indicates that the protofilaments wind around a hollow core<sup>20</sup>.

## Supplementary Results 2: Atomic Force Microscopy and Fluorescence Spectroscopy.

Atomic force microscopy (AFM) provides a means to image A $\beta$ 42 oligomers in a hydrated state without the need for negative staining. We had previously introduced a new approach for AFM measurements of A $\beta$  oligomers that images the particles using a low force single touch of the AFM probe per pixel<sup>5</sup>. The single touch AFM methodology has two advantages over conventional tapping mode AFM: the measurements are done in aqueous buffer and only low force contacts with the samples are made, minimizing disruption due to impact of the AFM tip. The height measurements by AFM are extremely accurate, whereas the width measurements require a correction based on the width of the AFM tip<sup>5</sup>. **Supplementary Figures 2a and 2b** present representative fields of A $\beta$ 42 oligomers obtained by single touch AFM.

AFM was carried out using a LifeScan controller developed by LifeAFM (Port Jefferson, NY) interfaced with a Digital Instruments (Santa Barbara, CA) MultiMode microscope fitted with an E scanner. With this instrument configuration, only a single contact of the AFM probe is made with the sample per pixel with minimal compressive forces (30–100 piconewtons nm<sup>-1</sup>) applied to the sample. AFM samples were prepared by adsorbing 20  $\mu$ L of sample mixture to freshly cleaved ruby mica (S & J Trading, Glen Oaks, NY). Samples were imaged under hydrated conditions using super-sharp silicon probes (SSS-Cont, Nanosensors, Neuchatel, Switzerland) that were modified for magnetic retraction by attaching samarium cobalt particles. We estimate the effective diameter of the super-sharp silicon probes to be  $4 \pm 1$  nm at a height of 2 nm. For volumetric estimates, non-overlapping particles in several fields were analyzed with different dilution. Data analysis and graphics was performed using Interactive Display Language 5.0 (Research Systems Inc., Boulder, CO). In the Z-scale bars, numbers in each color square indicate the Z-value at the middle of the range for that color.

To monitor the stability of A $\beta$ 42 oligomers prepared under low salt and low temperature conditions, thioflavin T binding was monitored by fluorescence spectroscopy. Thioflavin T fluorescence has been widely used to characterize the kinetics of fibril formation<sup>27</sup>. The thioflavin T molecule exhibits an increase in fluorescence intensity at 490 nm when bound to A $\beta$  fibrils. Binding of thioflavin T to A $\beta$  oligomers does not induce a change in fluorescence, allowing the fluorescence measurements to be a quantitative measure of fibril formation. **Supplementary Figure 2e** shows the fluorescence intensity change as a function of incubation time for A $\beta$ 42 peptides at low salt conditions at 4 °C and 37 °C.

### Height analysis of A $\beta$ 42 oligomers

In **Supplementary Figure 2c**, there are two distributions of heights measured from the resolved particles in **Supplementary Figure 2b**. The first distribution has a maximum at 2.2 nm. The second distribution has a maximum between 3 and 4 nm. No particles are observed with heights between 0.75 and 1.2 nm in **Supplementary Figure 2b**. Intensity that occurs in just one or a

few pixels with a height below 0.75 nm is considered noise. The average height and standard deviation of 183 particles in **Supplementary Figure 2b** is 2.2 nm and 0.72 nm, respectively. We have previously observed that the particles with heights of ~4 nm can be capped by the addition of peptide inhibitors without changing their width<sup>19</sup>. If the particles with heights of ~2 nm represent the pentamers and hexamers that have been identified by Teplow and co-workers through cross-linking studies<sup>28</sup>, then particles with heights of ~4 nm would be consistent with dodecamers observed by mass spectroscopy<sup>6</sup> and other methods<sup>29</sup>.

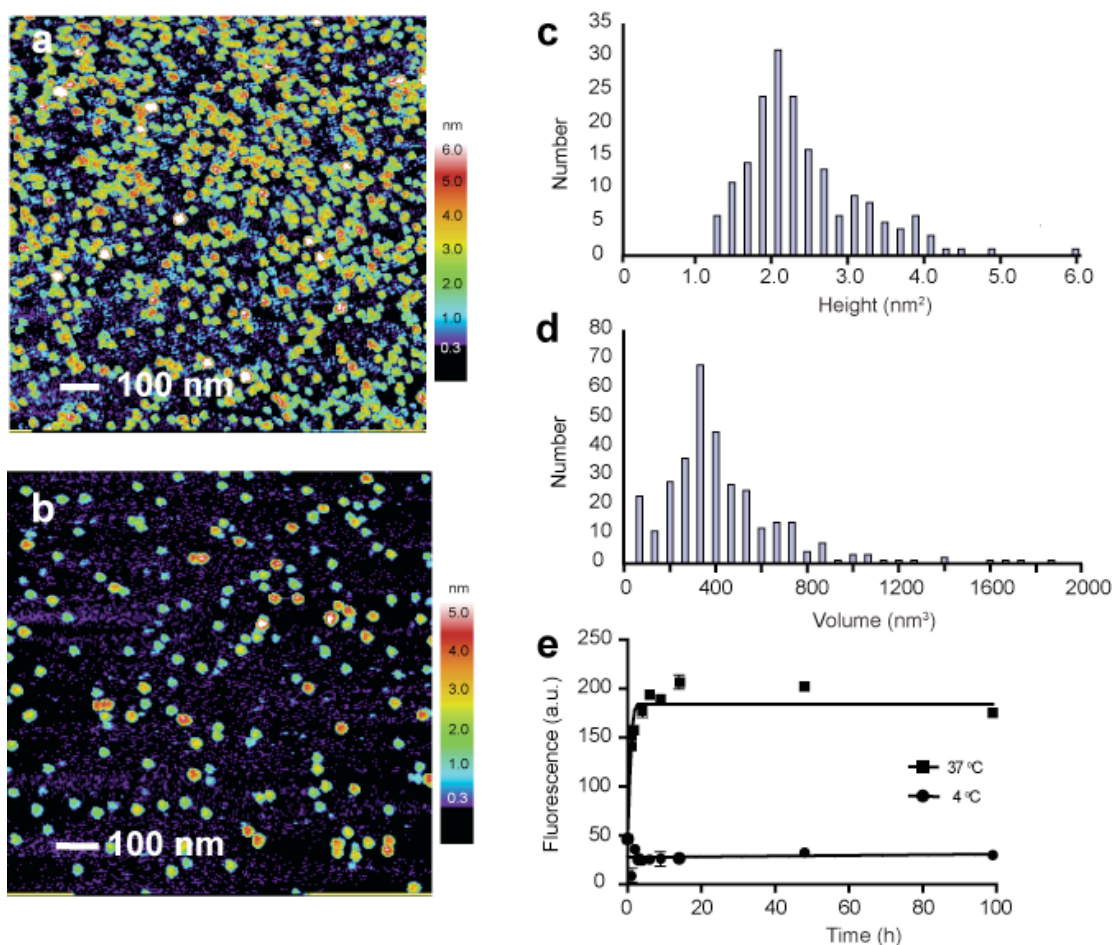
### **Volumetric analysis of A $\beta$ 42 oligomers**

In **Supplementary Figure 2d**, the volumes of non-overlapping particles observed in the AFM field of view for **Supplementary Figures 2a-b** can be calculated from their heights and corrected widths. The histogram of particle volumes suggests there are three separate distributions of particles. The first distribution corresponds to monomers/dimers with volumes of less than 100 nm<sup>3</sup>. We have previously arrayed the soluble oligomers formed from A $\beta$ 42 by size and height (see Figure 2 in Mastrangelo *et al.*<sup>5</sup>). The smallest particles observed had heights of 1–1.5 nm and widths of 5–7 nm, which we categorized as monomers or dimers. The second distribution corresponds to pentamers with a mean volume of ~ 350 nm<sup>3</sup>. A volume of 350 nm<sup>3</sup> is equivalent to a cylinder with a radius of 7.1 nm and a height of 2.2 nm. Visually, this distribution corresponds to the most numerous oligomers observed in **Supplementary Figure 2b** with blue/green height coloring. The third distribution corresponds to decamers or dodecamers with a volume of ~ 700 nm<sup>3</sup>, twice the size of 350 nm<sup>3</sup> particles. This distribution corresponds to the oligomers with orange/red height coloring. The oligomers are disc-shaped, rather than spherical micelles, i.e. the widths of the A $\beta$ 42 oligomers are appreciably greater than the heights.

We can estimate the number of individual monomers/dimers in the oligomer sample as ~3% of the total number of monomers by analyzing the height or volume distributions and assuming monomers/dimers have heights of 0.75–1.5 nm and volumes of < 200 nm<sup>3</sup> (see Mastrangelo *et al.*<sup>5</sup>). Similarly, we can estimate the number of large oligomers with volumes greater than ~1000 nm<sup>3</sup> to be less than 1% on the basis of their relatively numbers.

### **Time-resolved binding of thioflavin T to A $\beta$ 42 oligomers incubated at 4 °C and 37 °C**

Oligomer samples are stable at 4 °C for several days. The same samples incubated at 37 °C rapidly form fibrils with a very short lag phase due to the relatively high concentration (200  $\mu$ M) of A $\beta$ 42 peptide used (see sample preparation methods in main text). Thioflavin T binding assays were performed for A $\beta$ 42 oligomer samples incubated at 4 °C and 37 °C. Thioflavin T dye was added to A $\beta$ 42 samples at a 20:1 ratio, and fluorescence was measured at 490 nm with an excitation wavelength of 446 nm in a SpectraMax spectrofluorometer (Molecular Devices, Sunnyvale, CA) using SoftMax Pro control software.



**Supplementary Figure 2.** Representative images are shown after incubation of A $\beta$ 42 for 6 h (a) and 72 h (b) at 4 °C. The images were collected after dilution of a 150  $\mu$ M solution by a factor of 15 for the 6 h time point and by a factor of 50 for the 72 h time point. The image obtained at the 6 h time point and a concentration of 10  $\mu$ M reveals that that particles are relatively homogeneous with respect to their width, consistent with TEM images shown in Figure 2 (main text). The image obtained at the 72 h time point and at a lower concentration contains mostly non-overlapping particles, although the particle sizes are comparable to those observed at 6 h. The resolution allows us to estimate the size (height and volume) of the particles in this sample. (c) Height analysis of A $\beta$ 42 oligomers. (d) Volume analysis of A $\beta$ 42 oligomers. (e) Time resolved thioflavin T binding of A $\beta$ 42 oligomer samples incubated at 4 °C and 37 °C. The size distribution of the oligomers did not change over 100 h of incubation.

### Supplementary Results 3: Size Exclusion Chromatography and Dynamic Light Scattering.

Size exclusion chromatography (SEC) has been used extensively for characterizing the size distributions of oligomers of A $\beta$  peptides under nondenaturing, nondisaggregating conditions<sup>30,31</sup>. The method is useful for distinguishing protofibrils from small oligomers, and in some cases has the ability to distinguish smaller populations of oligomers. **Supplementary Figure 3** presents an analysis by SEC of the A $\beta$ 42 oligomers stabilized at 4 °C under low salt conditions in order to estimate their composition and homogeneity. Additionally, dynamic light scattering measurements were taken of the A $\beta$ 42 oligomer samples and are described below.

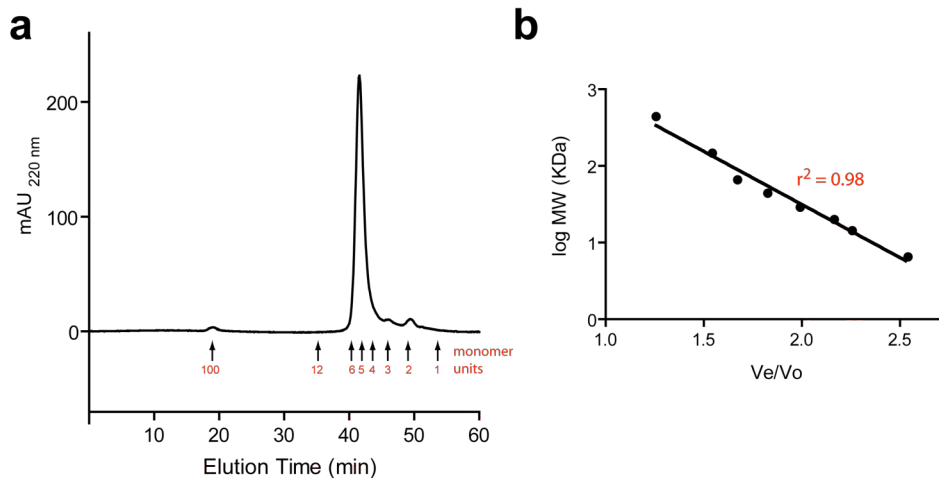
The two methods, SEC and AFM, for estimating the composition and purity of the sample are not readily comparable. However, there are some general conclusions that can be drawn. First, the level of monomers/dimers in the sample estimated by both methods is small, on the order of 2-3% of the total. Second, the level of very large oligomers is small, again less than ~2% of the total. Taken together, the AFM and SEC results agree that over 90% of the sample is comprised of small oligomers from pentamers to dodecamers. The SEC results and the AFM results are not completely consistent with respect to the distribution of small oligomers (pentamers to dodecamers). The SEC analysis shows a relatively narrow distribution for the predominant oligomer that migrates with a molecular weight corresponding to a pentamer (and possibly hexamer). In contrast, our analysis of AFM heights suggests the presence of two distributions of particles. The major fraction of the particles observed by AFM has heights of ~2 nm and molecular volumes corresponding to pentamers/hexamers. A minor fraction of the particles observed by AFM has heights of 3–4 nm and molecular volumes corresponding to decamers/dodecamers. Both populations of particles have the similar widths (10-15 nm) suggesting that the 2 nm high particles (i.e. pentamers) can associate in solution. We propose that the absence of decamers (or dodecamers) in the SEC (and native gel) measurements is due to weak association of the pentamers under low temperature and low salt conditions.

A $\beta$ 42 oligomer samples were analyzed by size exclusion chromatography using an ÄKTA Purifier 10 FPLC (GE Healthcare, Piscataway, NJ) placed in a deli-case refrigerator at 4 °C. Samples were injected into a Superdex 200 column (3000 – 600,000 MW range) at an elution rate of 0.4 ml min<sup>-1</sup> and detected by absorbance at 220 nm. A standard calibration curve (**Supplementary Figure 3b**) was constructed by measuring elution times of ferritin (440 kDa), alcohol dehydrogenase (150 kDa), bovine serum albumin (66 kDa), ovalbumin (44 kDa), carbonic anhydrase (29 kDa), soybean trypsin inhibitor (20 kDa), lysozyme (14 kDa), and aprotinin (6.5 kDa).

### Dynamic Light Scattering

Dynamic light scattering has been used to study the initial aggregation kinetics of A $\beta$  peptides since the amount of scattering increases exponentially with the size of the particle<sup>30,32</sup>. The drawback of dynamic light scattering is that the exponential dependence of the scattering intensity on particle size means that a few, large aggregates in the sample can overwhelm the scattering from smaller, more abundant species. Nevertheless, dynamic light scattering can provide an estimate of the hydrated radius of the particle if the larger aggregates are removed. Measurements were taken of A $\beta$ 42 oligomers stabilized by low temperature and low salt before and after filtering through a 0.02  $\mu$ m filter. Unfiltered samples had average diameters of 98.6 nm (0.327 polydispersity), whereas filtered samples had average diameters of 14.8 nm (0.375 polydispersity). The SEC analysis of the A $\beta$ 42 oligomers showed that in addition to the dominant pentamer/hexamer complex, a very weak larger complex of ~100 monomers was observed. This small contribution of a large aggregate dominates the light scattering from the sample and results in a very large effective particle. However, when the sample is filtered, the result is an oligomer diameter that matches that obtained from AFM.

Dynamic light scattering measurements were made using a Brookhaven Instruments 90Plus Particle Size Analyzer (Brookhaven Instruments, Holtsville, NY). A $\beta$ 42 oligomer samples were prepared as described in the main text or with an additional filtering step using a 0.02  $\mu$ m nylon filter (PALL Microelectronics, East Hills, NY).



Peak	Elution Time (min)	Integration	Elution Volume (mL)	Calculated MW (KDa)	Monomer units
1	19.02	1.2%	7.61	890 $\pm$ 100	200 $\pm$ 20
2	41.57	94%	16.63	24 $\pm$ 3	5.4 $\pm$ 0.6
3	45.73	2.6%	18.29	13 $\pm$ 1	2.9 $\pm$ 0.2
4	49.44	2.0%	19.78	8 $\pm$ 1	1.8 $\pm$ 0.2

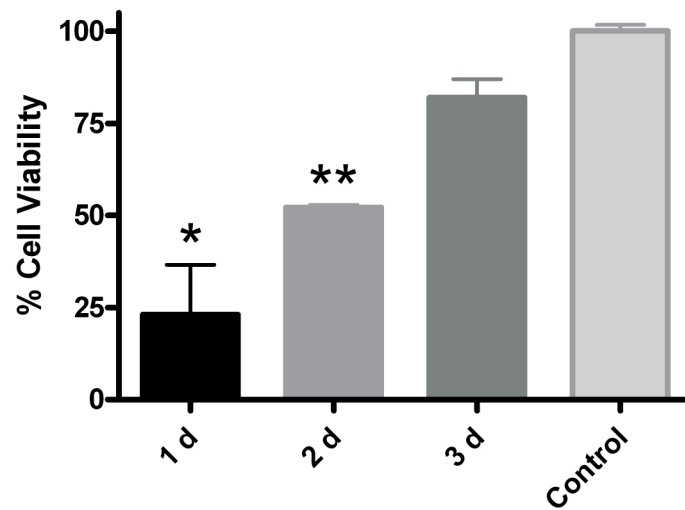
**Supplementary Figure 3.** Size exclusion chromatography of A $\beta$ 42 oligomers. The SEC chromatogram in **(a)** shows a single intense peak indicating that the majority of particles (94%) have molecular weights corresponding to a pentamer/hexamer complex. Small percentages of trimers and dimers, as well as higher order complexes, are also present. No monomers are present. The use of low salt and low temperature in the SEC may contribute to improving the resolution. In **(b)**, a standard calibration curve is presented with an  $r^2$  value of 0.98. The observation of smaller oligomeric species supports the use of a standard calibration curve in analyzing particle sizes and supports the conclusion that the particles observed by single-touch AFM are relatively homogeneous.

#### Supplementary Results 4: Toxicity and Cell-Viability Assays.

Several cell culture models have been used to assay  $\beta$ -amyloid toxicity, including PC12<sup>33-35</sup>, neuroblastoma<sup>36-39</sup>, and primary murine neuronal cultures<sup>40-42</sup>. Primary cultures of murine cortical neurons were chosen for this study because they closely resemble the human neuronal environment. Cell viability was determined by assaying mitochondrial reduction of the tetrazolium redox dye 3-(4,5-dimethylthiazol-2-yl)-2,5-diphenyltetrazolium bromide (MTT). MTT reduction has been shown to be a reliable and reproducible indicator of the cytotoxic potential of A $\beta$  peptides<sup>43</sup>. In **Figure 2f** (main text), we showed the effects of toxicity on primary neuronal cells by the addition of soluble oligomers formed at low temperature and low salt conditions and of protofibrils (and oligomers) after incubation at 37 °C for 6 h. In **Supplementary Figure 4**, we extend these studies to show that the toxicity of A $\beta$ 42 decreases further as the oligomers/protofibrils are incubated for longer time periods (1-3 days) under physiological salt conditions before adding to the neuronal cell cultures. Under these conditions, mature fibrils are formed, and the population of neurotoxic oligomers diminishes.

Neonatal murine cortical neuronal cultures were prepared using 6-8 E16 pups. Prior to culture, 48-well plates were incubated overnight at 4°C with 4  $\mu\text{g ml}^{-1}$  laminin (Sigma, St. Louis, MO) and 100  $\mu\text{g ml}^{-1}$  poly-D-Lysine (Sigma, St. Louis, MO). The plates were rinsed with sterile water and allowed to dry under UV light. Under sterile conditions, the pups were extracted from the uterus of a decapitated female, their brains removed and placed into chilled Hank's BSS without  $\text{Ca}^{2+}$  and  $\text{Mg}^{2+}$  (Invitrogen, Carlsbad, CA). The brain stem, olfactory bulbs, and leptomeninges were removed from each brain. The HBSS was replaced with Neurobasal medium (Invitrogen, Carlsbad, CA) containing 0.25% trypsin and the tissue was incubated at 37 °C for 10–15 min. The tissue was washed 3x with plain Neurobasal medium followed by 10 min, room temperature incubation in Neurobasal medium containing 2  $\text{mg ml}^{-1}$  soybean trypsin inhibitor (Sigma, St. Louis, MO). The tissue was washed 3x with plain Neurobasal medium. The tissue was dispersed using three fire polished decreasing size borehole Pasteur pipettes in G3 Neurobasal medium containing 10  $\mu\text{g/ml}$  gentamicin (Sigma, St. Louis, MO), 25  $\mu\text{M}$  L-glutamate, 500  $\mu\text{M}$  L-glutamine (Invitrogen, Carlsbad, CA) and B27 (Invitrogen, Carlsbad, CA), followed by filtration through a 40  $\mu\text{m}$  cell strainer (Fisher Scientific, Waltham, MA). The volume of the filtered cell suspension was increased to 25 ml with G3 medium. The filtered suspension was left undisturbed for 5-10 min after which 10 ml of filtered suspension was removed from the top and placed into a new tube. 10 ml of G3 medium was added back into the filtered cell suspension and this procedure was repeated two more times. The 30 ml of collected cell suspension was centrifuged 200 x g for 2 min and the supernatant removed. The cell pellet was re-suspended in 1 ml G3 medium. The cells were counted and plated at  $6.7 \times 10^5$  cells/ml in two 24-well plates. On day two, one half of the G3 medium was removed from the cell cultures and replaced with the same volume of fresh G3 medium. On day three, one half of the medium was removed and replaced with the same volume of G2 Neurobasal medium containing 10  $\mu\text{g}$

ml<sup>-1</sup> Gentamicin, 500 μM L-glutamine, B27, and 10 μM araC (Cytosine-β-F-arabinofuranoside) (Sigma, St. Louis, MO). All experiments were performed between days 4-6 using G2 medium without araC.



**Supplementary Figure 4.** Cell viability assay of primary cultures of murine cortical neurons treated with Aβ42 peptides incubated under physiological salt conditions (10 mM phosphate, 150 mM NaCl, pH 7.4) at 37 °C for 1, 2, or 3 d (n=3) before the addition to the neuronal cell cultures. Results represent the mean ± sem, \* p < 0.05, \*\* p < 0.01.

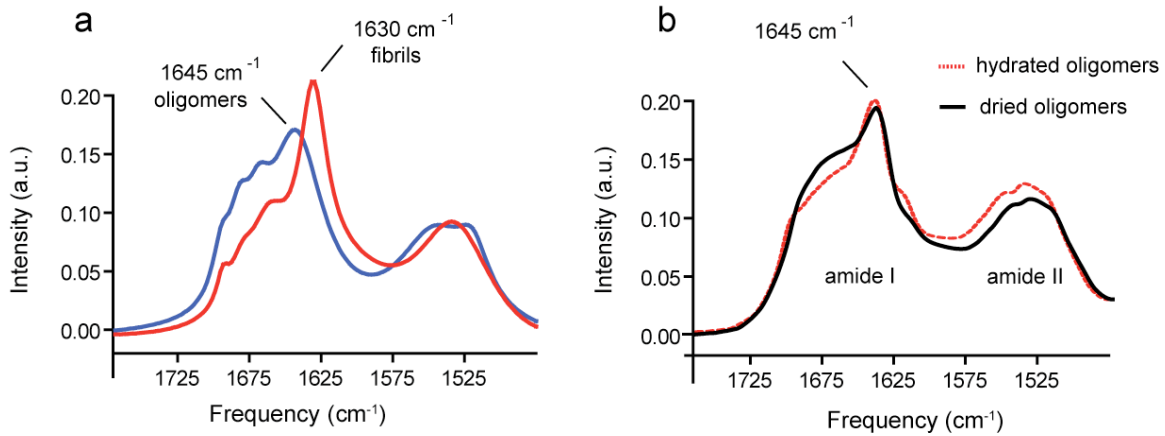
## Supplementary Results 5: Fourier Transform Infrared (FTIR) Spectroscopy.

FTIR<sup>44,45</sup>, Raman<sup>46</sup> and CD<sup>47,48</sup> spectroscopy have been used extensively to assess the secondary structure of A $\beta$  fibrils and oligomers. Raman and IR methods monitor the amide vibrational frequencies, which are sensitive to secondary structure. **Supplementary Figure 5** presents the FTIR spectra of A $\beta$ 42 fibrils and oligomers. In **Supplementary Figure 5a**, the IR spectrum of the fibrils is dominated by an amide I vibration at 1630 cm<sup>-1</sup>, characteristic of  $\beta$ -sheet secondary structure<sup>49</sup>. The integrated intensity of this band suggests that most (85%) of the fibril structure is  $\beta$ -sheet. The amide I intensities are consistent with the model proposed in **Supplementary Figure 1** where only the N-terminal 10 amino acids are solvent exposed. The N-terminal residues are thought to be unstructured. In the IR spectrum, random coil is observed as a broad featureless band at ~1650 cm<sup>-1</sup>. The region from 1660–1695 cm<sup>-1</sup> has several distinct (i.e. narrow) bands that may be attributed to the turn structure in the fibrils and to side chain vibrations of arginine, asparagine and glutamine.

The IR spectrum of the stable oligomers (blue) is distinctly different from that of the fibrils. There is a relatively well-defined band at 1645 cm<sup>-1</sup>. This band is broader than the corresponding band for the fibrils, but still too low in frequency to correspond to  $\alpha$ -helix. We assign the 1645 cm<sup>-1</sup> vibrational band to unordered secondary structure and/or to ‘aggregated strand’ that has a less defined preference for  $\phi$  and  $\psi$  torsion angles. There is increased intensity in the amide I region from 1660-1695 cm<sup>-1</sup> relative to the fibrils. We assign the vibrational modes in this region to turns in the A $\beta$ 42 sequence and side chain vibrations of arginine, asparagine and glutamine. The solvent accessibility studies described in **Supplementary Results 6** suggest there are more turns in the oligomers than fibrils. We do not assign the high frequency vibration at 1685 cm<sup>-1</sup> to anti-parallel  $\beta$ -sheet structure<sup>45</sup> on the basis of the H/D exchange and volumetric analysis of the AFM images.

**Supplementary Figure 5b** presents FTIR spectra of hydrated (red dashed line) and lyophilized (black line) oligomers. The major component of the spectrum at 1645 cm<sup>-1</sup> has the same frequency and intensity indicating that the overall conformation is not influenced by lyophilization. There is a small increase in intensity between 1660 and 1685 cm<sup>-1</sup> and a small decrease in intensity at 1620 cm<sup>-1</sup> upon lyophilization that we attribute to small changes in the interaction of the N-terminal sequence of the A $\beta$ 42 peptide upon lyophilization.

The FTIR spectra were obtained from 400–4000 cm<sup>-1</sup> on a Bruker IFS 66V/S spectrometer. The spectral area from 1425 to 1900 cm<sup>-1</sup> were curve fit and the integral values of the fitting curves were used to determine the amount of  $\beta$  sheet, random coil,  $\alpha$  helix,  $\beta$  turn, and anti-parallel  $\beta$  sheet contributions to the peptide structure. Different secondary structures have characteristic amide frequencies as shown<sup>49</sup>.

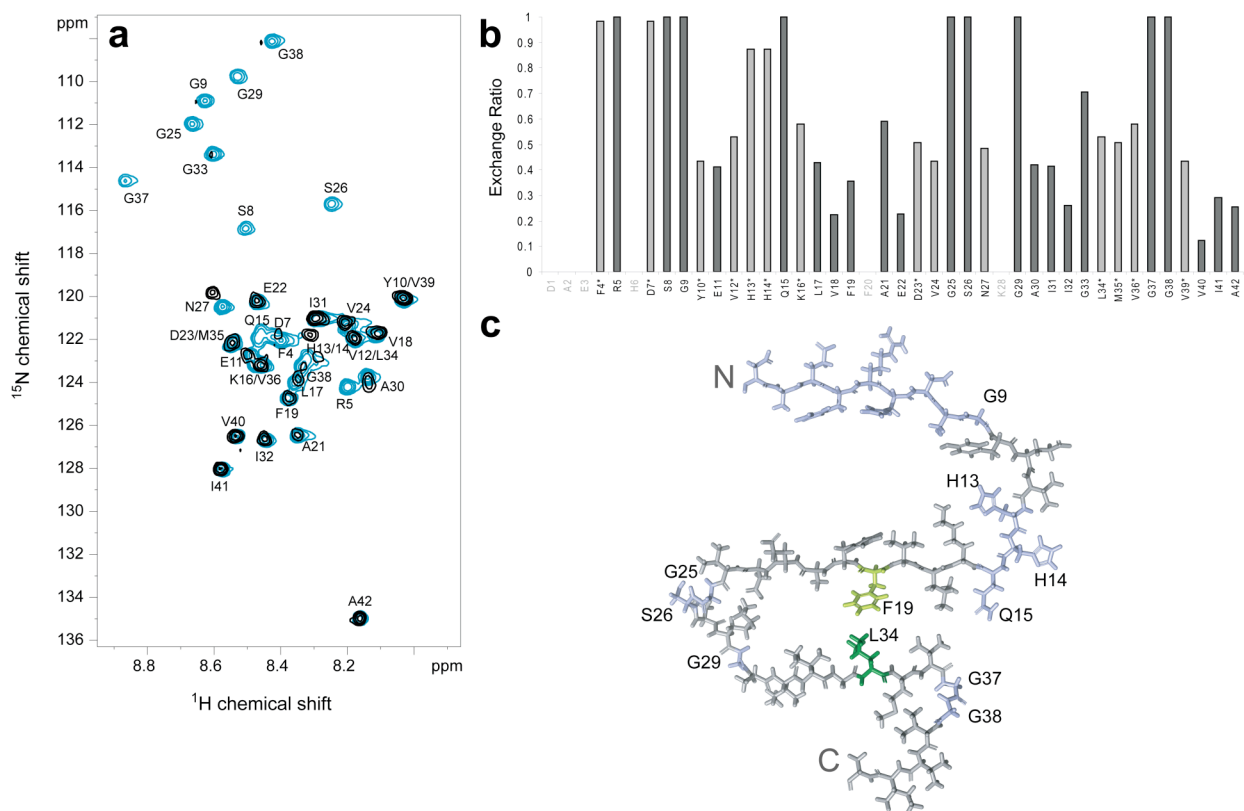


	Oligomers	Fibrils
1610-1640 cm <sup>-1</sup> β-sheet/aggregated strands	44%	85%
1648-1660 cm <sup>-1</sup> α-helix/unordered	27%	14%
1660-1685 cm <sup>-1</sup> Turns	19%	3.3%
1675-1695 cm <sup>-1</sup> Anti-parallel β-sheet aggregated strands Arg, Asn, Gln side-chains	11%	1.7%

**Supplementary Figure 5.** (a) FTIR spectra are presented of the Aβ<sub>42</sub> oligomers (blue) and fibrils (red). (b) FTIR spectra of hydrated (red dashed line) and lyophilized (black line) oligomers.

## Supplementary Results 6: Amide Hydrogen-Deuterium Exchange by Solution NMR Spectroscopy.

The soluble nature, stable character and relatively low molecular weight of the neurotoxic oligomers makes them amenable to solution NMR methods. Previous studies on monomers of A $\beta$ 42 have yielded assignments for the resonances observed in the  $^1\text{H}$ - $^{15}\text{N}$  heteronuclear single quantum coherence (HSQC) spectra<sup>47,50,51</sup>. **Supplementary Figure 6** takes advantage of these assignments to probe the solvent accessibility as a function of the A $\beta$ 42 sequence.



**Supplementary Figure 6. Solvent accessibility of A $\beta$ 42 oligomers.** (a)  $^1\text{H}$ - $^{15}\text{N}$  heteronuclear single quantum coherence (HSQC) spectra of A $\beta$ 42 oligomers in 10% D<sub>2</sub>O, 90% H<sub>2</sub>O (blue) and 70% D<sub>2</sub>O, 30% H<sub>2</sub>O (black) to measure amide hydrogen-deuterium (H-D) exchange. Several peaks completely exchange indicating regions of high solvent accessibility.

(b) Exchange ratios calculated for each residue showing distinct regions of solvent accessibility and protection. Peaks with overlapping assignments are marked with (\*) and the exchange ratios are colored in light gray. No peak assignments were made for Asp1, Ala2, Glu3, His6, Phe20, or Lys28.

(c) Schematic of A $\beta$ 42 monomer in the oligomer conformation based on solid-state NMR and amide H-D exchange. In addition to the turn conformation defined by the Phe19-Leu34 contact observed by solid-state DARR NMR measurements, amide exchange

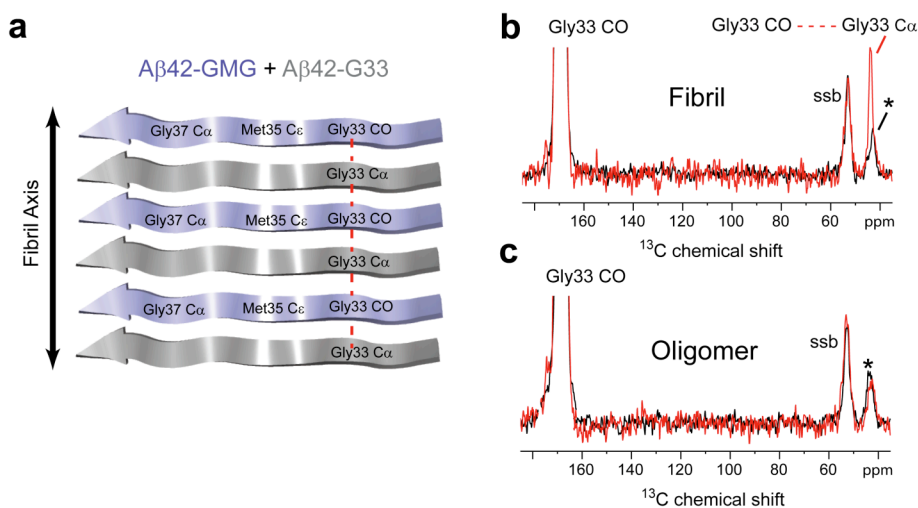
suggests solvent accessible turn regions at His13-Gln15, Gly25-Gly29, and Gly37-Gly38, as well as a loosely defined solvent accessible N-terminal segment up to Gly9.

Oligomer samples were prepared using U-<sup>15</sup>N-A $\beta$ 42 peptides (rPeptide, Bogart, GA) and analyzed on a Bruker AVANCE 700 MHz spectrometer using a TXI probe. <sup>1</sup>H-<sup>15</sup>N HSQC spectra were obtained at 4 °C on A $\beta$ 42 oligomer samples containing either 10% D<sub>2</sub>O (for signal locking) or 70% D<sub>2</sub>O (for exchange). Peak assignments were based on previous reports<sup>47,50,51</sup>. Peak exchange occurred within the experimental acquisition time (< 1.5 h) and exchange ratios were calculated as the ratio of the deconvoluted peak volumes of the exchanged samples (containing 70% D<sub>2</sub>O) relative to the deconvoluted peak volumes of the non-exchanged samples (containing 10% D<sub>2</sub>O).

## Supplementary Results 7: Additional Distance Constraints in A $\beta$ 42 Fibrils and Oligomers by Solid State NMR Spectroscopy.

Additional DARR constraints were obtained on A $\beta$ 42 fibrils using the peptides listed in **Table 1** of the main text. No internuclear  $^{13}\text{C}\dots^{13}\text{C}$  cross-peaks were observed between the following residues: His13/14-Gly33, His13/14-Met35, His13/14-Gly37, His13/14-Ala42, Gln15-Val39, Gln15-Ala42, Phe19-Gly37, Phe19-Gly38, Ile31-Gly37, Ile31-Val39, and Gly33-Val39.

**Supplementary Figure 7** provides an additional structural constraint at Gly33 on the strand orientation of A $\beta$ 42 fibrils and oligomers.



**Supplementary Figure 7.** Parallel and in-register orientation of  $\beta$ -strands in A $\beta$ 42 fibrils, but not in neurotoxic oligomers. **(a)** Labeling scheme to test for a parallel and in-register orientation of the C-terminal  $\beta$ -strand in A $\beta$ 42 fibrils and oligomers using an equimolar mixture of A $\beta$ 42-GMG and A $\beta$ 42-G33 peptides. The red dashed line corresponds to the 4.7 Å distance expected between adjacent Gly33 residues along the fibril axis. **(b)** Rows from the two dimensional DARR spectra of A $\beta$ 42 fibrils formed from an equimolar mixture of A $\beta$ 42-GMG:A $\beta$ 42-G33 (red trace) or A $\beta$ 42-GMG alone (black trace). A large cross-peak (red line) is observed in the A $\beta$ 42-GMG:A $\beta$ 42-G33 mixture indicating inter-strand molecular contacts between Gly33-CO and Gly33-C $\alpha$  in a parallel and in-register orientation. A smaller natural abundance (\*) cross-peak is observed in the spectrum of A $\beta$ 42-GMG alone. Spinning side bands (ssb) are observed due to magic angle spinning as indicated. **(c)** Rows from the two dimensional DARR spectra of A $\beta$ 42 oligomers formed from an equimolar mixture of A $\beta$ 42-GMG:A $\beta$ 42-G33 peptides (red trace) or from A $\beta$ 42-GMG peptide alone (black trace). No change in cross-peak intensity is observed, indicating that C-terminal strands in A $\beta$ 42 oligomers do not have a parallel and in-register orientation.

**Supplementary Table 1. <sup>13</sup>C Chemical Shifts of Aβ42 Oligomers and Fibrils.**

<sup>13</sup>C NMR chemical shifts (ppm relative to neat tetramethylsilane) of Aβ42 oligomers and fibrils. For split assignments, the major chemical shifts (>70%) are shown in bold.

	<b>Aβ42 oligomers</b>	<b>Aβ42 fibrils</b>
<b>His13/14</b> Cε <sub>1</sub>	136.0	136.1
<b>Gln15</b> Cδ	176.4	176.0
<b>Phe19</b> Cγ Cδ <sub>1</sub> , Cδ <sub>2</sub> , Cε <sub>1</sub> , Cε <sub>2</sub> , Cζ	137.1 129.1	137.1 128.7
<b>Ala21</b> CO Cα	173.0 48.6	<b>174.1</b> , 173.0 <b>50.8</b> , 48.4
<b>Ile31</b> CO Cα Cβ Cγ <sub>1</sub> Cγ <sub>2</sub> Cδ	174.9, <b>170.9</b> <b>60.4</b> , 55.0 36.1 26.0 15.5 12.0	<b>177.2</b> , 170.1 <b>61.2</b> , 53.4 41.4, <b>38.0</b> 25.8 14.4 12.5
<b>Gly33</b> CO Cα	168.9 44.6	169.2 44.0
<b>Leu34</b> CO Cα Cβ Cγ, Cδ <sub>1</sub> , Cδ <sub>2</sub>	<b>174.6</b> , 166.5 58.0, <b>50.0</b> 44.3 24.4	<b>173.7</b> , 167.3 57.4, <b>50.2</b> 42.6 24.9
<b>Met35</b> Cε	15.4	17.2, 15.3 (1:1)
<b>Gly37</b> CO Cα	169.9 43.3	169.4 42.9
<b>Gly38</b> Cα	43.6	46.7, <b>41.8</b>
<b>Val39</b> CO Cα Cβ Cγ <sub>1</sub> , Cγ <sub>2</sub>	173.4 58.2 33.8 19.0	176.8, <b>170.5</b> <b>60.7</b> , 53.7 34.1 18.9
<b>Ala42</b> Cβ	19.7	19.9

## References

1. Lashuel, H.A. & Lansbury, P.T. Are amyloid diseases caused by protein aggregates that mimic bacterial pore-forming toxins? *Q. Rev. Biophys.* **39**, 167-201 (2006).
2. Lesné, S. et al. A specific amyloid- $\beta$  protein assembly in the brain impairs memory. *Nature* **440**, 352-357 (2006).
3. Lambert, M.P. et al. Diffusible, nonfibrillar ligands derived from A $\beta$ <sub>1-42</sub> are potent central nervous system neurotoxins. *Proc. Natl. Acad. Sci. U.S.A.* **95**, 6448-6453 (1998).
4. Gellermann, G.P. et al. A $\beta$ -globulomers are formed independently of the fibril pathway. *Neurobiol. Dis.* **30**, 212-220 (2008).
5. Mastrangelo, I.A. et al. High-resolution atomic force microscopy of soluble A $\beta$ 42 oligomers *J. Mol. Biol.* **358**, 106-119 (2006).
6. Bernstein, S.L. et al. Amyloid- $\beta$  protein oligomerization and the importance of tetramers and dodecamers in the aetiology of Alzheimer's disease. *Nature Chemistry* **1**, 326-331 (2009).
7. Chen, Y.R. & Glabe, C.G. Distinct early folding and aggregation properties of Alzheimer amyloid- $\beta$  peptides A $\beta$ 40 and A $\beta$ 42 - Stable trimer or tetramer formation by A $\beta$ 42. *J. Biol. Chem.* **281**, 24414-24422 (2006).
8. Urbanc, B. et al. In silico study of amyloid  $\beta$ -protein folding and oligomerization. *Proc. Natl. Acad. Sci. U.S.A.* **101**, 17345-17350 (2004).
9. Yun, S.J. et al. Role of electrostatic interactions in amyloid  $\beta$ -protein (A $\beta$ ) oligomer formation: A discrete molecular dynamics study. *Biophys. J.* **92**, 4064-4077 (2007).
10. Nguyen, P.H., Li, M.S., Stock, G., Straub, J.E. & Thirumalai, D. Monomer adds to preformed structured oligomers of A $\beta$ -peptides by a two-stage dock-lock mechanism. *Proc. Natl. Acad. Sci. U.S.A.* **104**, 111-116 (2007).
11. Kirschner, D.A., Abraham, C. & Selkoe, D.J. X-ray-diffraction from Intraneuronal paired helical filaments and extraneuronal amyloid fibers in Alzheimer-disease indicates cross- $\beta$  conformation. *Proc. Natl. Acad. Sci. U.S.A.* **83**, 503-507 (1986).
12. Balbach, J.J. et al. Supramolecular structure in full-length Alzheimer's  $\beta$ -amyloid fibrils: Evidence for a parallel  $\beta$ -sheet organization from solid-state nuclear magnetic resonance. *Biophys. J.* **83**, 1205-1216 (2002).
13. Antzutkin, O.N., Leapman, R.D., Balbach, J.J. & Tycko, R. Supramolecular structural constraints on Alzheimer's  $\beta$ -amyloid fibrils from electron microscopy and solid-state nuclear magnetic resonance. *Biochemistry* **41**, 15436-15450 (2002).
14. Torok, M. et al. Structural and dynamic features of Alzheimer's A $\beta$  peptide in amyloid fibrils studied by site-directed spin labeling. *J. Biol. Chem.* **277**, 40810-40815 (2002).
15. Lührs, T. et al. 3D structure of Alzheimer's amyloid- $\beta$ (1-42) fibrils. *Proc. Natl. Acad. Sci. U.S.A.* **102**, 17342-7 (2005).

16. Olofsson, A., Sauer-Eriksson, A.E. & Ohman, A. The solvent protection of Alzheimer amyloid- $\beta$ -(1-42) fibrils as determined by solution NMR spectroscopy. *J. Biol. Chem.* **281**, 477-483 (2006).
17. Masuda, Y. et al. Verification of the C-terminal intramolecular  $\beta$ -sheet in A $\beta$ 42 aggregates using solid-state NMR: Implications for potent neurotoxicity through the formation of radicals. *Bioorg. Med. Chem. Lett.* **18**, 3206-3210 (2008).
18. Morimoto, A. et al. Analysis of the secondary structure of  $\beta$ -amyloid (A $\beta$  42) fibrils by systematic proline replacement. *J. Biol. Chem.* **279**, 52781-52788 (2004).
19. Sato, T. et al. Inhibitors of amyloid toxicity based on  $\beta$ -sheet packing of A $\beta$ 40 and A $\beta$ 42. *Biochemistry* **45**, 5503-5516 (2006).
20. Zhang, R. et al. Interprotofilament interactions between Alzheimer's A $\beta$ <sub>1-42</sub> peptides in amyloid fibrils revealed by cryoEM. *Proc. Natl. Acad. Sci. U.S.A.* **106**, 4653-4658 (2009).
21. Meinhardt, J., Sachse, C., Hortschansky, P., Grigorieff, N. & Fändrich, M. A $\beta$ (1-40) fibril polymorphism implies diverse interaction patterns in amyloid fibrils. *J. Mol. Biol.* **386**, 869-877 (2009).
22. Sachse, C., Fändrich, M. & Grigorieff, N. Paired  $\beta$ -sheet structure of an A $\beta$ (1-40) amyloid fibril revealed by electron microscopy. *Proc. Natl. Acad. Sci. U.S.A.* **105**, 7462-7466 (2008).
23. Paravastu, A.K., Qahwash, I., Leapman, R.D., Meredith, S.C. & Tycko, R. Seeded growth of  $\beta$ -amyloid fibrils from Alzheimer's brain-derived fibrils produces a distinct fibril structure. *Proc. Natl. Acad. Sci. U.S.A.* **106**, 7443-7448 (2009).
24. Paravastu, A.K., Leapman, R.D., Yau, W.M. & Tycko, R. Molecular structural basis for polymorphism in Alzheimer's  $\beta$ -amyloid fibrils. *Proc. Natl. Acad. Sci. U.S.A.* **105**, 18349-18354 (2008).
25. Sciarretta, K.L., Gordon, D.J., Petkova, A.T., Tycko, R. & Meredith, S.C. A $\beta$  40-Lactam(D23/K28) models a conformation highly favorable for nucleation of amyloid. *Biochemistry* **44**, 6003-6014 (2005).
26. Tycko, R. Molecular structure of amyloid fibrils: Insights from solid-state NMR. *Q. Rev. Biophys.* **39**, 1-55 (2006).
27. LeVine, H. Quantification of  $\beta$ -sheet amyloid fibril structures with thioflavin T. *Meth. Enzymol.* **309**, 274-284 (1999).
28. Bitan, G., Vollers, S.S. & Teplow, D.B. Elucidation of primary structure elements controlling early amyloid  $\beta$ -protein oligomerization. *J. Biol. Chem.* **278**, 34882-34889 (2003).
29. Frydman-Marom, A. et al. Cognitive-performance recovery of Alzheimer's disease model mice by modulation of early soluble amyloidal assemblies. *Angew. Chem. Int. Ed. Engl.* **48**, 1981-6 (2009).
30. Walsh, D.M., Lomakin, A., Benedek, G.B., Condron, M.M. & Teplow, D.B. Amyloid  $\beta$ -protein fibrillogenesis - Detection of a protofibrillar intermediate. *J. Biol. Chem.* **272**, 22364-22372 (1997).

31. Bitan, G. & Teplow, D.B. Preparation of aggregate-free, low molecular weight amyloid- $\beta$  for assembly and toxicity assays. *Methods Mol. Biol.* **299**, 3-9 (2005).
32. Lomakin, A., Chung, D.S., Benedek, G.B., Kirschner, D.A. & Teplow, D.B. On the nucleation and growth of amyloid  $\beta$ -protein fibrils: Detection of nuclei and quantitation of rate constants. *Proc. Natl. Acad. Sci. U.S.A.* **93**, 1125-1129 (1996).
33. Vaisid, T., Barnoy, S. & Kosower, N.S. Calpastatin overexpression attenuates amyloid- $\beta$ -peptide toxicity in differentiated PC12 cells. *Neuroscience* **156**, 921-931 (2008).
34. Diaz, J.C., Simakova, O., Jacobson, K.A., Arispe, N. & Pollard, H.B. Small molecule blockers of the Alzheimer A $\beta$  calcium channel potentially protect neurons from A $\beta$  cytotoxicity. *Proc. Natl. Acad. Sci. U.S.A.* **106**, 3348-3353 (2009).
35. Mruthinti, S., Capito, N., Sood, A. & Buccafusco, J.J. Cytotoxicity of A $\beta$ (1-42), RAGE(23-54), and an A $\beta$ -RAGE complex in PC-12 cells. *Curr. Alzheimer Res.* **4**, 581-586 (2007).
36. Picone, P. et al. A $\beta$  oligomers and fibrillar aggregates induce different apoptotic pathways in LAN5 neuroblastoma cell cultures. *Biophys. J.* **96**, 4200-4211 (2009).
37. Zameer, A., Kasturirangan, S., Emadi, S., Nimmagadda, S.V. & Sierks, M.R. Anti-oligomeric A $\beta$  single-chain variable domain antibody blocks A $\beta$ -induced toxicity against human neuroblastoma cells. *J. Mol. Biol.* **384**, 917-928 (2008).
38. Liu, R.T. et al. Single chain variable fragments against  $\beta$ -amyloid (A $\beta$ ) can inhibit A $\beta$  aggregation and prevent A $\beta$ -induced neurotoxicity. *Biochemistry* **43**, 6959-6967 (2004).
39. Austen, B.M. et al. Designing peptide inhibitors for oligomerization and toxicity of Alzheimer's  $\beta$ -amyloid peptide. *Biochemistry* **47**, 1984-1992 (2008).
40. Romito-DiGiacomo, R.R., Menegay, H., Cicero, S.A. & Herrup, K. Effects of Alzheimer's disease on different cortical layers: The role of intrinsic differences in A $\beta$  susceptibility. *J. Neurosci.* **27**, 8496-8504 (2007).
41. Cheng, J.S. et al. Collagen VI protects neurons against A $\beta$  toxicity. *Nat. Neurosci.* **12**, 119-121 (2009).
42. Hung, L.W. et al. Amyloid- $\beta$  Peptide (A $\beta$ ) neurotoxicity is modulated by the rate of peptide aggregation: A $\beta$  dimers and trimers correlate with neurotoxicity. *J. Neurosci.* **28**, 11950-11958 (2008).
43. Shearman, M.S. Toxicity of protein aggregates in PC12 cells: 3-(4,5-dimethylthiazol-2-yl)-2,5-diphenyltetrazolium bromide assay. *Meth. Enzymol.* **309**, 716-23 (1999).
44. Seshadri, S., Khurana, R. & Fink, A.L. Fourier transform infrared spectroscopy in analysis of protein deposits. *Meth. Enzymol.* **309**, 559-576 (1999).
45. Cerf, E. et al. Antiparallel  $\beta$ -sheet: a signature structure of the oligomeric amyloid  $\beta$ -peptide. *Biochem. J.* **421**, 415-23 (2009).
46. Eker, F., Griebenow, K. & Schweitzer-Stenner, R. A $\beta$ <sub>1-28</sub> fragment of the amyloid peptide predominantly adopts a polyproline II conformation in an acidic solution. *Biochemistry* **43**, 6893-6898 (2004).
47. Barrow, C.J. & Zagorski, M.G. Solution structures of  $\beta$  peptide and its constituent fragments: Relation to amyloid deposition. *Science* **253**, 179-182 (1991).

48. Tomaselli, S. et al. The  $\alpha$ -to- $\beta$  conformational transition of Alzheimer's A $\beta$ (1-42) peptide in aqueous media is reversible: A step by step conformational analysis suggests the location of  $\beta$  conformation seeding. *Chembiochem* **7**, 257-267 (2006).
49. Tamm, L.K. & Tatulian, S.A. Infrared spectroscopy of proteins and peptides in lipid bilayers. *Q. Rev. Biophys.* **30**, 365-429 (1997).
50. Olofsson, A., Sauer-Eriksson, A.E. & Öhman, A. Amyloid fibril dynamics revealed by combined hydrogen/deuterium exchange and nuclear magnetic resonance. *Anal. Biochem.* **385**, 374-376 (2009).
51. Olofsson, A., Lindhagen-Persson, M., Sauer-Eriksson, A.E. & Öhman, A. Amide solvent protection analysis demonstrates that amyloid- $\beta$ (1-40) and amyloid- $\beta$ (1-42) form different fibrillar structures under identical conditions. *Biochem. J.* **404**, 63-70 (2007).